Journal of Materials Chemistry

Cite this: J. Mater. Chem., 2011, 21, 15655

www.rsc.org/materials



PAPER

# Fabrication of a large scale transparent conducting film using transformed few-layered graphene nanoribbons obtained from unzipping of single wall carbon nanotubes

Woo Sik Kim,[a] Yong Il Kim,[b] Hui Jin Kim,[a] Ji Young Hwanag,[a] Sook Young Moon,[c] No-Hyung Park,[a] Kwang Bo Shim,[b] Hyoun Woo Kim,[b] Heon Ham[d] and Hoon Huh*[a]

*Received 16th May 2011, Accepted 2nd August 2011*
**DOI: 10.1039/c1jm12158h**



A large scale transparent conducting film has been fabricated using transformed few-layered graphene nanoribbons (FGNRs) obtained from unzipping of single wall carbon nanotubes and poly(3,4-ethylenedioxythiophene). FGNRs are fabricated from an unzipping process of single-walled carbon nanotubes with a high direct current pulse through a pulsed current sintering process. From control of the film thickness and conductivity, the optical transmittance values of films at a wavelength of 550 nm were 84% and 92%, and have sheet resistances of 150 and 2000 Ω $sq^{-1}$. High resolution transmission electron microscopy, high resolution Raman spectroscopy, X-ray photoelectron spectroscopy, transmittance and electrical conductivity were used for the investigation of the FGNRs and FGNR transparent electrodes to characterize the films.

## Introduction

Fabrication of a commercial transparent electrode is based on thin film technology and semiconductor processing methods. Although present commercial technology continues to be the material choice for current transparent electrode applications, the two-dimensional (2-D) nanostructure of graphene has been attracting much attention in recent years to be fabricated as the transparent electrode because of its high electric conductivity and reduction of cost compared to the conventional transparent electrode of indium tin oxide (ITO).[1–3]

Because graphene with atomic scale thickness has excellent transparency and electric conductivity properties, the prototype of the graphene-based flat panel transparent electrode has been fabricated.[1,4] Compared with the current ITO-based transparent electrode, the graphene-based transparent electrode could possibly substitute the ITO transparent electrode in the future due to its high electric transportation and transparent properties.

Graphene nanoribbon structures such as zigzag, armchair have been realized using several techniques including chemical vapor deposition, plasma etching and high pulsed current methods, *etc.*[1,5–7] As half-metal zigzag-edged graphene nanoribbons (GNRs)[8] and narrow band-gap armchair-edged graphene nanoribbons (GNRs) of 1–3 eV for 1–2 nm wide GNRs with a small binding energy (0.8–1.4 eV)[9] graphene-based 2-D nanostructures have received increasing attention over the past few years due to its potential applications in graphene field effect transistors (FETs),[10,11] newly introduced bilayer pseudo-spin field effect transistors (BiSFETs),[12] and transparent conductive electrodes.[1]

In this paper, we reported the fabrication of a transparent electrode on a glass substrate by simple spin-/spray-coating methods with the use of few-layered graphene nanoribbons (FGNRs) and poly(3,4-ethylenedioxythiophene). In this process, FGNRs were fabricated using a high direct current (DC) pulse under a pulse current sintering (PCS) process and single-walled carbon nanotubes (SWCNTs).[13] The number of layers and widths of FGNRs are controlled by SWCNTs. The structures and electrical properties of the transparent electrode were investigated. And also the transparency of the transparent electrode was investigated.

## Experimental method

The SWCNTs (Hanwha Nanotech, ASP-100F, Korea) were synthesized using transition metals (Co, Ni, Fe, or their mixture) and the arc-discharge method. The SWCNTs consist not only of 90% of SWCNTs but also of a uniform distribution of diameters (1–2 nm) and length (5–20 μm). And also small (1–2 nm) metal particles are embedded in a capsule of SWCNTs, or aggregates and stick to the nanotube bundles. Therefore, SWCNTs were

[a]*Korea Institute of Industrial Technology, 35-3 HongCheon-ri Ipjang-myeon, Seobuk-gu, Cheonan-si, 331-825, Korea. E-mail: wskim@kitech.re.kr; Fax: +82-41-589-8360; Tel: +82-41-589-8355*
[b]*Division of Advanced Material Science and Engineering, Hanyang Univ., Seoul, 133-791, Korea*
[c]*Advanced Composite Group, Aerospace Research and Development Directorate (ARD), Japan Aerospace Exploration Agency, 6-13-1 Osawa, Mitaka, Tokyo, 181-0015, Japan*
[d]*H&H Co. LTD, Chungju National University, 50 Daehak-ro, Chungju-si, Chungbuk, 330-702, Korea*

purified by acidic and thermal treatment, and also SWCNTs were centrifuged and rinsed with water for several times and dried in air. The content of metals (Co, Fe, Ni, or their mixture) in both acid residues was found to be less than 0.001%.

FGNRs were fabricated using SWCNTs and high pulse current in the PCS process. The pellets of FGNRs were produced in vacuum (mechanical pump) using a Dr sinter® model SPS-515S PCS system (Sumitomo Coal mining Co., Japan). Contacts were placed between two graphite rams in a cylindrical graphite (ISO-63) die having an inner diameter of 10 mm with 1 g SWCNTs. The pellets were heated to 2000 °C at a heating rate of 100 °C per minute with a pressure of 100 MPa between the rams, and the applied DC was about 700 A (voltage < 5 V) with a pulse duration of 12 ms and a pulse interval of 2 ms for 10 min. They are finally subjected to scanning electron microscopy, with a field emission gun (FE-SEM) for observation using a FEI-Nova NanoSEM200 instrument. High resolution transmission electron microscopy (HR-TEM) investigations were carried out using a JEOL-4010 microscope operating at 400 kV. Raman spectra were taken at room temperature under ambient conditions using a Lab Ram HR (Jobin-Yvon) with a laser excitation of 514.5 nm (Ar-ion laser). Also, X-ray photoelectron spectroscopy (XPS) used the VG Multilab ESCA 2000 system. The current–voltage ($I$–$V$) characteristics of the FGNRs and their comparisons were measured by the two probe method within an applied voltage ranging from −1.0 to 1.0 V using a source meter (Keithley Model 2400, OH, USA). In order to exclude the metal substrate, samples were measured on a glass wafer using a Pt-electrode. And, the FGNR transparent electrode is fabricated by the spray-/spin-coating process. UV transmittance measurements of FGNRs were performed using a UV-vis spectrophotometer (UV-2400, Shimadzu, Japan) from 400 to 700 nm of the visible light region. The sheet resistance of the FGNR electrode was analyzed using a four-point probe (CMT-SR-3000L4G, Changmin tech., Korea).

## Results and discussion

A pictorial representation of the transformation from SWCNTs to FGNRs under the high pulse current flow on the surface of SWCNTs is illustrated in Fig. 1. PCS is a field activated sintering technique based on the electrical spark discharge phenomenon, in which a high-energy and low-voltage sparking pulse current momentarily generates spark plasma at localized high temperatures. During the PCS process, a high DC pulse flows on the surface of the SWCNTs (Fig. 1a), and simultaneously $sp^2$ carbon bond breaking starts at one end of the SWCNT following the current direction. This phenomenon leads to the breakage of C–C bonds along the current path (Fig. 1b). The broken SWCNTs in a straight line were spread out by curvature tension on the surface of the SWCNT and then transformed into the graphene layer.[13] The transformed mono-layered graphene nanoribbons (MGNRs) have a large surface area (the theoretical surface area of an individual carbon sheet can be up to 2630–2965 $m^2\ g^{-1}$).[14,15] The individual carbon sheet could not exist in a planar structure because of the large surface area.[16] Thus, to reduce the large surface area, they are combined promptly by van der Waals force. The combined graphenes are stacked on each other, and then form the few-layered structure (Fig. 1c).[17] We prepared the

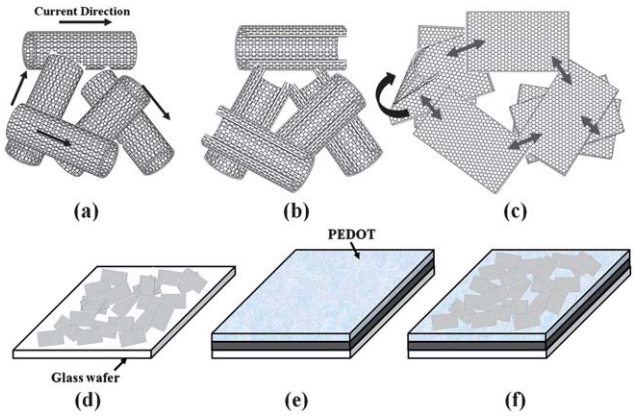


**Fig. 1** Illustration of the transformation model of SWCNTs to FGNRs by high pulse current unzipping and fabrication process for the FGNR electrode: (a) disordered SWCNTs as starting materials before current flow, (b) unzipped SWCNTs along the current path, (c) SWCNTs spread out by curvature tension. To reduce the surface energy, they became stacked on top of each other because of van der Waals force, (d) FGNRs are spray- or spin-coated on a glass wafer, (e) PEDOT was spray- or spin-coated, and (f) the deposition of FGNRs was repeated (in the case of the spray coating process).

dispersion solution of FGNRs in ethanol solvent (FGNR/ethanol = 1/1000 weight ratio). The FGNR solution was spray-coated on a glass wafer at a density of 0.0625–0.25 ml $cm^{-2}$. Or, this solution was deposited on a glass wafer by spin-coating at from 1000 to 4000 rpm for 60 s (Fig. 1d). After drying, to increase the electrical network among FGNRs, the conductive polymer such as poly(3,4-ethylenedioxythiophene) (PEDOT, Aldrich) was deposited on the FGNR coated glass wafer by spin- or spray-coating (Fig. 1e). To increase the electrical conductivity of the transparent electrode, we repeated the deposition process of FGNRs on the FGNR/PEDOT coated substrate (Fig. 1f). Table 1 shows the number of deposited layers on glass wafers and their concentration.

Fig. 2a shows HR-TEM images of GNRs. The stacked several GNRs are confirmed. The width of the GNR is about 4.2 nm (the inset of Fig. 2a, upper right), which is unzipped from the SWCNT with a diameter of about 1.5 nm (the inset image of Fig. 2a, upper left). The edge of the GNR is formed in a curling up structure, such as a nanotube or a nano-scroll. This phenomenon proves that the GNR is fabricated by unzipping of the SWCNT and stretched by curvature tension. Fig. 2b shows the cross-section of FGNRs. Because of MGNRs, the thickness of FGNRs is about 1–3 atomic layers. The inset images reveal that the interlayer space of the bi- or triple-layer graphene is the same as 0.34 nm of the ideal graphite. And the length of unzipped SWCNTs is several micrometres, which is similar with pristine SWCNTs.[17]

Fig. 3a shows Raman spectra for FGNRs, as well as for SWCNTs. These spectra primarily show four Raman bands at ~165 $cm^{-1}$ (RBM), ~1355 $cm^{-1}$ (D band), ~1585 $cm^{-1}$ (G band) and ~2707 $cm^{-1}$ (2nd order band).[18] The G band occurs because of the original graphite features, and in plane vibration of $sp^2$ carbon atoms. The D band peak, which has been known to occur because of amorphous carbon, contains a certain fraction of $sp^3$ carbon.[19] The intensity ratio of the D band to the G band ($I_D/I_G$)



 

**Table 1** Summary of SWCNT/PEDOT and FGNR/PEDOT based electrodes

| Spray coating | | Spin coating |
|---|---|---|
| SWCNT-based electrode | FGNR-based electrode | FGNR-based electrode |
| S: SWCNT solution<br>(SWCNT/ethanol = 1/1000 wt%)<br>P: PEDOT solution<br>(PEDOT/ethanol = 1/5 wt%)<br>S1: S/P film<br>(SWCNT solution: 0.0625 ml $cm^{-2}$)<br>S2: S/P/S film<br>(SWCNT solution: 0.125 ml $cm^{-2}$)<br>S3: S/P/S/S/S film<br>(SWCNT solution: 0.25 ml $cm^{-2}$) | F: FGNR solution<br>(FGNR/ethanol = 1/1000 wt%)<br>P: PEDOT solution<br>(PEDOT/ethanol = 1/5 wt%)<br>F1: F/P film<br>(FGNR solution: 0.0625 ml $cm^{-2}$)<br>F2: F/P/F film<br>(FGNR solution: 0.125 ml $cm^{-2}$)<br>F3: F/P/F/F/F film<br>(FGNR solution: 0.25 ml $cm^{-2}$) | F: FGNR solution<br>(FGNR/ethanol = 1/1000 wt%)<br>P1: PEDOT solution<br>(PEDOT/ethanol = 1/10 wt%)<br>1000–4000 rpm: F/P1 films |



and the proportion of their dimensions have been used for evaluation factor of the in-plane crystallite in the graphite structure.[20,21] The value of $I_D/I_G$ for the starting material is 0.11. This demonstrates that our starting material has very good crystallinity.[22] However, after transformation to the graphene layer with high current DC pulses, the value of $I_D/I_G$ is increased up to 0.85. Commonly, the increase of the intensity ratio $I_D/I_G$ is caused by structural defects of the graphitic structure.[23] However, the sharpness of D and 2D bands of FGNRs is not decreased comparing with pristine SWCNTs. The full width at half maximum (FWHM) of FGNRs at D and 2D bands is 37 $cm^{-1}$ and 56 $cm^{-1}$. And the FWHM of pristine SWCNTs at D and 2D bands is 62 $cm^{-1}$ and 44 $cm^{-1}$. And, the electrical conductivity of FGNRs is higher than SWCNTs (Fig. 5b). Therefore, the increase of D band intensity at FGNRs is due to the edges of GNRs, not caused by the structural defects.[24,25] The radial breathing mode (RBM) at 150–200 $cm^{-1}$ of SWCNTs has disappeared after the high current DC pulses have been applied, showing the transformation from a 1D tubular structure to a 2D planar structure.[26] The intensity of the 2D band at 2600–2700 $cm^{-1}$ serves to establish the electric conductivity in the carbon material and to determine the number of layers in graphene.[18,27,28] The value of $I_{2D}/I_G$ is increased from 0.17 to 0.94, showing that the mixture of semiconducting and metallic electrical properties in SWCNTs changes to a metallic state because of transformation of the graphene layer.[27] The C1s XPS spectrum of FGNR is shown in Fig 3b. The binding energy of the C–C $sp^2$ bond is assigned to 284.6 eV, as it was in the starting material. Also, we do not find chemical shifts at +1.5, +2.5 and +4.0 eV, which would typically occur for typical C–OH, C=O, and O=C–OH functional groups of graphene oxides.[29,30] Furthermore, the binding energy of $sp^3$ carbon, such as in a diamond structure, is not found.[31,32] The crystal has become an amorphous structure whenever the same peak spectrum of the crystal becomes too broad.[31] However, the sharpness of C1s spectra at FGNR is not changed, in comparison with the starting material. This XPS result reveals that the transformed GNRs by high pulse current unzipping have the same $sp^2$ carbon structure when SWCNTs are the starting materials. Also, the increase of intensity of the D band in the Raman spectrum of FGNRs does not indicate a shift of the carbon structure into an amorphous, $sp^3$ or a functional carbon state. These results prove that FGNRs are not the structure of graphene oxide.

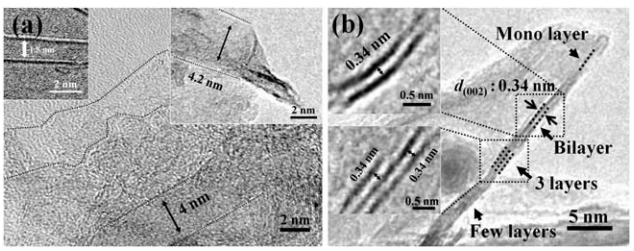


**Fig. 2** (a) HR-TEM images of GNRs; the insets show SWCNTs as the starting materials (upper left) and the enlarged individual GNR (upper right), and (b) the cross-sections of FGNRs; insets show the interlayer space of GNRs.

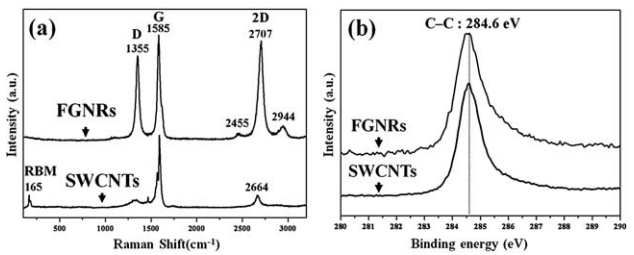


**Fig. 3** (a) Raman spectra at 514 nm, and (b) XPS spectra of FGNRs. The comparison is made with purified SWCNTs.

Fig. 4 shows the transmittance and sheet resistance of SWCNT- and FGNR-based electrodes. The spray-coated SWCNT-based electrodes on the PEDOT (0.0625 ml $cm^{-2}$) coated glass wafer with various contents of SWCNTs (S1–3) have the transmittance of 90–92% at a wavelength of 550 nm (Fig 4a). But, their sheet resistances are about 8500–10 000 Ω $sq^{-1}$, which are similar to the pristine PEDOT film (Fig 4d, P; black dot—transmittance: 92.66% at 550 nm, sheet resistance: 10 580 Ω $sq^{-1}$). These results reveal that SWCNT-based electrodes had very good transmittance, but could not get an increase of electrical conductivity by addition of SWCNTs. The thickness of FGNRs is larger than the diameter of SWCNTs by the stacking of MGNRs, therefore the spray-coated FGNR-based electrodes have lower transmittance (84–92% at a wavelength of 550 nm) compared to SWCNT-based electrodes (Fig 4b). But, by increasing the FGNR concentration, the sheet resistance of FGNR-based electrodes is dramatically decreased up to 600 Ω $sq^{-1}$ (Fig. 4d, F1–3; blue line). Fig. 4c shows the

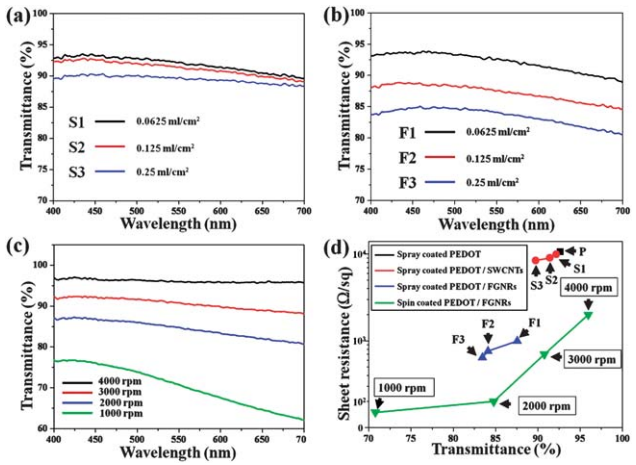


**Fig. 4** (a) Transmittance of SWCNT-based electrodes, which were fabricated by spray coating at various concentrations of the SWCNT solution, (b) transmittance of FGNR-based electrodes, which were fabricated by spray coating at various concentrations of the FGNR solution, (c) transmittance of FGNR-based electrodes, which were prepared at different spin coating rates from 1000 to 4000 rpm, (d) sheet resistance and transmittance (at a wavelength of 550 nm) of the pristine PEDOT, the spray-coated SWCNT-based electrode, the spray-coated FGNR-based electrode and the spin-coated FGNR-based electrode.

transmittance of spin-coated FGNR-based electrodes. By increasing a spin-coating rate from 1000 to 4000 rpm, the transmittance is increased from 71 to 96% at a wavelength of 550 nm. And the sheet resistance of spin-coated FGNR-based electrodes shows 150–2000 Ω $sq^{-1}$ (Fig. 4d, green line), which is proportional to transmittance.

Fig. 5a shows the FGNR-based electrodes on a glass wafer with a size of 10 × 10 $cm^2$. To examine the electrical conductivity of FGNRs, we measured the current–voltage characteristic. As can be seen in Fig. 5b, all samples exhibit a linear *I–V* relation within the experimental conditions (from −1.0 to 1.0 V). The left inset of Fig. 5b shows the Pt patterned electrical device and its enlarged electrode image. The distance between two electrodes is 3 micrometres and the width of electrode is 3 micrometres.

The SWCNTs have the lowest slope in the *I–V* curve, which indicates a lower electrical conductivity than the others. It is well known that SWCNTs were formed into various structures, such as zigzag, armchair and chiral. These mixed structures caused the mixture of semiconducting and metallic electrical properties of SWCNTs. By unzipping SWCNTs, SWCNTs change to a metallic state because of transformation of the graphene layer. The *I–V* slope of SWCNTs is increased by transformation to FGNRs. However, after transformation, the local disorder has been created by high DC pulse and high temperature. This local disorder leads to the decrease of the *I–V* slope compared with highly ordered pyrolytic graphite (HOPG). This result reveals that transformation of SWCNTs to FGNRs is an advantageous way to enhance its conductivity.

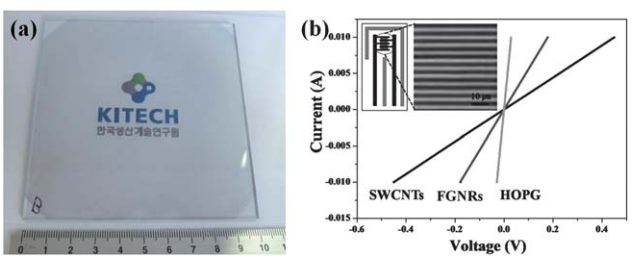


**Fig. 5** (a) A digital image of the FGNR-based electrode on a glass wafer (10 × 10 $cm^2$) with KITECH logo underneath, and (b) current–voltage curves of FGNRs. The comparisons are between HOPG and SWCNTs; the micro-patterned Pt-electrode (inset).

## Conclusions

We have transformed SWCNTs into FGNRs using high pulse current unzipping in the PCS process. We can fabricate a fixed number of layers of GNR uniform in width by using SWCNTs with uniform distribution of diameters as starting materials. In addition, we confirmed that MGNRs are not present as individual sheets, because of the effects of their high surface energy. To reduce the surface area, they have become stacked on top of one another to form FGNR structures with 2–3 layers. And its electrical conductivity is increased compared to starting materials. The fabrication method of GNRs using high current DC pulses can produce FGNRs more quickly than in the previous methods without oxidation. And, the FGNR-based electrode has excellent transparency and sheet resistivity compared to the SWCNT-based electrode. Therefore, the pulse current unzipping and fabrication of the FGNR-based electrode technique show great potential in the fabrication of GNRs and their commercial applications.

## Notes and references

1 K. S. Kim, Y. Zhao, H. Jang, S. Y. Lee, J. M. Kim, K. S. Kim, J. H. Ahn, P. Kim, J. Y. Choi and B. H. Hong, *Nature*, 2009, **457**, 706–710.
2 P. Blake, P. D. Brimicombe, R. R. Nair, T. J. Booth, D. Jiang, F. Schedin, L. A. Ponomarenko, S. V. Morozov, H. F. Gleeson, E. W. Hill, A. K. Geim and K. S. Novoselov, *Nano Lett.*, 2008, **8**, 1704–1708.
3 X. Wang, L. Zhi and K. Müllen, *Nano Lett.*, 2008, **8**, 323–327.
4 X. Li, Y. Zhu, W. Cai, M. Borysiak, B. Han, D. Chen, R. D. Piner, L. Colombo and R. S. Ruoff, *Nano Lett.*, 2009, **9**, 4359–4363.
5 K. S. Novoselov, A. K. Geim, S. V. Morozov, D. Jiang, Y. Zhang, S. V. Dubonos, I. V. Grigorieva and A. A. Firsov, *Science*, 2004, **306**, 666.
6 Y. B. Zhang, Y. W. Tan, H. L. Stormer and P. Kim, *Nature*, 2005, **438**, 201.
7 X. Li, X. Wang, L. Zhang, S. Lee and H. Dai, *Science*, 2008, **319**, 1229.
8 M. Wu, X. Wu, Y. Gao and X. C. Zeng, *Appl. Phys. Lett.*, 2009, **94**, 223111.
9 Y. Li, L. C. Marvin and S. G. Louie, *Nano Lett.*, 2007, **7**, 3112–3115.
10 S. Kim, J. Nah, I. Jo, D. Shahrjerdi, L. Colombo, Z. Yao, E. Tutuc and S. K. Banerjee, *Appl. Phys. Lett.*, 2009, **94**, 062107.
11 M. C. Lemme, T. J. Echtermeyer, M. Baus, B. N. Szafranek, J. Bolten, M. Schmidt, T. Wahlbrink and H. Kurz, *Solid-State Electron.*, 2008, **52**, 514–518.
12 S. K. Banerjee, L. F. Register, E. Tutuc, D. Reddy and A. H. MacDonald, *IEEE Electron Device Lett.*, 2009, **30**, 158–160.
13 W. S. Kim, S. Y. Moon, S. Y. Bang, B. G. Choi, H. Ham, T. Sekino and K. B. Shim, *Appl. Phys. Lett.*, 2009, **95**, 083103.
14 A. Peigney, C. Laurent, E. Flahaut, R. R. Bacsa and A. Rousset, *Carbon*, 2001, **39**, 507–514.
15 H. K. Chae, D. Y. Siberio-perez, J. Kim, Y. B. Go, M. Eddaoudi, A. J. Matzger, O. Michael and M. Y. Omar, *Nature*, 2004, **427**, 523–527.
16 M. V. Lisa, J. M. Julia and B. K. Ricard, *Science*, 2006, **299**, 1361.
17 W. S. Kim, S. Y. Moon, N.-H. Park, H. Huh, K. B. Shim and H. Ham, *Chem. Mater.*, 2011, **23**, 940–944.

 

18 S. Reich and C. Thomsen, *Philos. Trans. R. Soc., A*, 2004, **362**, 2271–2288.
19 A. C. Ferrari, J. C. Meyer, V. Scardaci, C. Casiraghi, M. Lazzeri, F. Mauri, S. Piscanec, D. Jiang, K. S. Novoselov, S. Roth and A. K. Geim, *Phys. Rev. Lett.*, 2006, **97**, 187401.
20 F. Tuinstra and J. L. Koenig, *J. Chem. Phys.*, 1970, **53**, 1126–1230.
21 D. S. McClloch, S. Prawer and A. Hoffman, *Phys. Rev. B: Condens. Matter*, 1994, **50**, 5905–5917.
22 S. Osswald, E. Flahaut and Y. Gototsi, *Chem. Mater.*, 2006, **18**, 1525–1533.
23 P. Tan, S. L. Zhang, K. T. Yue and F. Huang, *J. Raman Spectrosc.*, 1997, **28**, 369–372.
24 C. Casiraghi, A. Hartschuh, H. Qian, S. Piscanec, C. Georgi, A. Fasoli, K. S. Novoselov, D. M. Basko and A. C. Ferrari, *Nano Lett.*, 2009, **9**, 1433–1441.
25 Z. Sun, T. Hasan, F. Torrisi, D. Popa, G. Privitera, F. Wang, F. Bonaccorso, D. M. Basko and A. C. Ferrari, *ACS Nano*, 2010, **4**, 803–810.
26 H. Kuzmany, W. Plank, M. Hulman, Ch. Kramberger, A. Gruneis, Th. Pichler, H. Peterlik, H. Kataura and Y. Achiba, *Eur. Phys. J. B*, 2001, **22**, 307–320.
27 K. K. Kim, J. S. Park, S. J. Kim, H. Z. Geng, K. H. An, C. M. Ynag, K. Sato, R. Saito and Y. H. Lee, *Phys. Rev. B: Condens. Matter Mater. Phys.*, 2007, **76**, 205426.
28 Y. Y. Wang, Z. H. Ni, Z. X. Shen, H. M. Wang and Y. H. Wu, *Appl. Phys. Lett.*, 2008, **92**, 043121.
29 H. Jeong, Y. P. Lee, R. J. W. E. Lahaye, M. Park, K. H. An, I. J. Kim, C. W. Yang, C. Y. Park, R. S. Ruoff and Y. H. Lee, *J. Am. Chem. Soc.*, 2008, **130**, 1362–1366.
30 D. Yang, A. Velamakanni, G. Bzoklu, S. Park, M. Stoller, R. D. Piner, S. Stankovich, I. Jung, D. A. Field, C. A. Ventrice, Jr and R. S. Ruoff, *Carbon*, 2009, **47**, 145–152.
31 Y. Kawabata, J. Taniguchi and I. Miyamoto, *Diamond Relat. Mater.*, 2004, **13**, 93–98.
32 R. M. Dey, M. Pandey, D. Bhattachryya, D. S. Patil and S. K. Kulkarni, *Bull. Mater. Sci.*, 2007, **30**, 541–546.